Available online at www.sciencedirect.com

SCIENCE DIRECT®

ELSEVIER

Journal of Computational Physics xxx (2005) xxx–xxx

JOURNAL OF COMPUTATIONAL PHYSICS

www.elsevier.com/locate/jcp

A level-set method for interfacial flows with surfactant

Jian-Jun Xu [a,*], Zhilin Li [b], John Lowengrub [c], Hongkai Zhao [c]

[a] *Department of Mathematics, Simon Fraser University, Burnaby, BC, Canada V5A 1S6*
[b] *Center for Scientific Computations and Department of Mathematics, North Carolina State University, Raleigh, NC 27695, USA*
[c] *Department of Mathematics, University of California at Irvine, Irvine, CA 92697, USA*

Received 31 March 2005; received in revised form 12 July 2005; accepted 15 July 2005

Abstract

A level-set method for the simulation of fluid interfaces with insoluble surfactant is presented in two-dimensions. The method can be straightforwardly extended to three-dimensions and to soluble surfactants. The method couples a semi-implicit discretization for solving the surfactant transport equation recently developed by Xu and Zhao [J. Xu, H. Zhao. An Eulerian formulation for solving partial differential equations along a moving interface, J. Sci. Comput. 19 (2003) 573–594] with the immersed interface method originally developed by LeVeque and Li and [R. LeVeque, Z. Li. The immersed interface method for elliptic equations with discontinuous coefficients and singular sources, SIAM J. Numer. Anal. 31 (1994) 1019–1044] for solving the fluid flow equations and the Laplace–Young boundary conditions across the interfaces. Novel techniques are developed to accurately conserve component mass and surfactant mass during the evolution. Convergence of the method is demonstrated numerically. The method is applied to study the effects of surfactant on single drops, drop–drop interactions and interactions among multiple drops in Stokes flow under a steady applied shear. Due to Marangoni forces and to non-uniform Capillary forces, the presence of surfactant results in larger drop deformations and more complex drop–drop interactions compared to the analogous cases for clean drops. The effects of surfactant are found to be most significant in flows with multiple drops. To our knowledge, this is the first time that the level-set method has been used to simulate fluid interfaces with surfactant.

AMS: 65M06; 65M12; 76T05

Keywords: Incompressible Stokes flow; Interfaces; Insoluble surfactant; Marangoni force; Capillary force; Level set method; Immersed interface method

[*] Corresponding author.
E-mail addresses: jxu@pims.math.ca, jianjunx@cs.sfu.ca (J.-J. Xu), zhilin@math.ncsu.edu (Z. Li), lowengrb@math.uci.edu (J. Lowengrub), zhao@math.uci.edu (H. Zhao).

0021-9991/$ - see front matter © 2005 Elsevier Inc. All rights reserved.
doi:10.1016/j.jcp.2005.07.016

1. Introduction

In this paper, we propose a level-set/immersed interface method for the evolution of deformable fluid interfaces with insoluble surfactant in two-dimensions. The method can be straightforwardly extended to three-dimensions and to soluble surfactants. Surfactants are surface-active molecules that selectively adhere to interfaces. Surfactants typically consist of a hydrophilic head and a hydrophobic tail – detergents are common examples. Surfactants play a critical role in numerous important industrial and biomedical applications ranging from enhanced oil recovery (e.g. [42]) to pulmonary function (e.g. [16]).

Surfactants are advected and diffused along interfaces by the motion of the fluid and by molecular mechanisms, respectively [9]. The surface tension depends on the surfactant distribution through the equation of state – regions of higher surfactant concentration have lower surface tension. Non-uniform surfactant concentration along an interface creates non-uniform Capillary (normal) and Marangoni (tangential) forces in the fluid. This in turn affect the fluid velocity that then couples back to affects the surfactant distribution. For example, the convection of surfactant toward the stagnation points at the tip of a drop tends to lower the surface tension there and increase the drop deformation. On the other hand, Marangoni forces resist the convection of surfactant toward the drop tip and thus restrain the deformation of the drop. Compression/stretching of the interface results in a corresponding increase/decrease in the surfactant concentration.

Computing the motion of interfacial flows with surfactant is challenging. The Navier–Stokes equations must be solved in a complex, multiply connected moving domain with prescribed jumps in the normal (Capillary) and the tangential (Marangoni) stress across the interface separating the domains. The moving interface must be accurately simulated and topology transitions may occur as interfaces reconnect or break-up. Further, as surfactant is advected and diffused along the interface there may be adsorption/desorption of surfactant from/to the bulk to/from the interface [9]. For simplicity, we focus here on the case of insoluble surfactant so that the surfactant remains bound to the interface.

In this paper, a level-set method for the simulation of fluid interfaces with insoluble surfactant is presented in two-dimensions. The method couples a semi-implicit discretization for solving the surfactant transport equation recently developed by Xu and Zhao [62] with the immersed interface method originally developed by LeVeque and Li [31] for solving the fluid flow equations and the Laplace–Young boundary conditions across the interfaces. Novel techniques are developed to accurately conserve component (domain) volume and surfactant mass during the evolution. Convergence of the method is demonstrated numerically. The method is applied to study the effects of surfactant on single drops, drop–drop interactions and interactions among multiple drops in Stokes flow under a steady applied shear. Due to Marangoni forces and to non-uniform Capillary forces, the presence of surfactant results in larger drop deformations and more complex drop–drop interactions compared to the analogous cases for clean drops. The effects of surfactant are found to be most significant in flows with multiple drops. To our knowledge, this is the first time that the level-set method has been used to simulate fluid interfaces with surfactant.

There are now a number of different numerical methods that have been developed to simulate the motion of surface-tension mediated interfacial flows (e.g., see [26]). Popular approaches include boundary integral methods (e.g., see the reviews [20,48]) where the flow equations are mapped to the interface, front-tracking/continuum surface force (CSF) methods (e.g., see the reviews [15,47,60]) where the flow equations are solved in the volume domain, a separate mesh is used to describe the interface and nearly singular surface forces (continuum surface force) are introduced to approximate the singular surface tension force, volume-of-fluid/CSF methods (e.g., see the review [50]) where a volume-fraction function is used to identify the interface, level-set/CSF methods (e.g., see the reviews [43,44,51]) where the interface is characterized by the zero contour of a level-set function and phase-field methods where a concentration field is introduced to identify fluid components (e.g., see the review [3,25,64]). A number of hybrid methods now exist including level-set/volume-of-fluid methods [56,58], particle level-set methods [12,18], marker/volume-of-fluid methods [4] and level-contour front tracking methods [52].

In addition to CSF methods, other flow solvers have been developed that directly account for the Laplace–Young surface tension jump conditions without smoothing. Advantages of such an approach include (1) no introduction of intermediate non-physical states near the interface since the interface condition is sharp, (2) higher-order accuracy can be achieved as opposed to CSF based methods which are generally only first-order accurate. Methods without smoothing include the method developed by Helenbrook et al. [17], the ghost-fluid (GF) method (e.g. [13,38]) and the immersed interface method (IIM, e.g. [19,30,32,35]). These algorithms have the common feature that standard finite difference schemes are used at grid points away from interfaces while the finite difference schemes are modified at grid points near interfaces. In the GF algorithm, subcell resolution is used to mark the interface position and the values of discontinuous quantities are artificially extended to grid points neighboring the interface via extrapolation. A fully second-order accurate GF method for moving interfaces with geometric boundary conditions has recently been developed [40]. A fourth-order GF method for the Laplace and heat equations has also been developed recently [14]. In the IIM, which is the approach we use here together with a level-set method, a local coordinate system is introduced to explicitly incorporate jump conditions and discontinuous coefficients into second-order accurate finite difference schemes. Advantages of this approach include its high-order accuracy, the ease of implementation and the fact that fast solvers (e.g., the FFT) can be used to invert the discrete systems.

Despite the vast literature on studies of drops and interfaces in multiphase flows, there are relatively few works in which the effects of surfactants are incorporated. Much of the previous work on surfactants has utilized the boundary integral method for axisymmetric (e.g., see [11,41,55]) and 3D (e.g., see [33,48,63]) Stokes flows. Recently, CSF-based methods have been developed for interfacial flows with surfactants using immersed boundary/front tracking methods [5,22] and volume-of-fluid methods [10,21,49]. We remark that in [21], an algorithm was developed to conserve both component mass and surfactant mass and is capable of simulating an arbitrary equation of state for the surfactant.

Recently, Xu and Zhao in [62] and Adalsteinsson and Sethian [2] presented methodologies to simulate transport and diffusion along deformable interfaces in conjunction with a level-set method. In the former work, Xu and Zhao applied their algorithm to study specifically the evolution of surfactant although they did not couple their method to a flow solver. Several test cases were presented in [62] in which a velocity field is prescribed. Here, we build upon this work by coupling the transport algorithm of Xu and Zhao to an IIM flow solver. We introduce modifications to conserve component and surfactant mass and we examine the effects of non-uniform Capillary forces and Marangoni forces on the evolution of interfaces in Stokes flow.

The remainder of this paper is organized as follows. The governing equations are presented in Section 2. The numerical method is described in Section 3, which includes the IIM for solving incompressible Stokes flow and the evolution schemes for the surfactant concentration and the level-set function. Numerical simulations are presented in Section 4 to illustrate the performance of the method. Conclusions and future directions are discussed in Section 5.

2. The governing equations

2.1. The Navier–Stokes equations

Consider an incompressible two-phase flow consisting of fluids 1 and 2 in a fixed domain $\Omega = \Omega_1 \cup \Omega_2$ where an interface Σ separates Ω_1 from Ω_2. In each region, the Navier–Stokes equations govern the fluid motion

$$\rho_i\left(\frac{\partial \mathbf{u}_i}{\partial t} + (\mathbf{u}_i \cdot \nabla)\mathbf{u}_i\right) = (\nabla \cdot \mathbf{T}_i)^{\mathrm{T}} + \rho_i \mathbf{g} \text{ in } \Omega_i \tag{1}$$

and

$$\nabla \cdot \mathbf{u}_i = 0 \text{ in } \Omega_i, \tag{2}$$

where $i = 1, 2$ denotes the fluid region, $\mathbf{T}_i = -p_i I + \mu_i(\nabla\mathbf{u}_i + \nabla\mathbf{u}_i^{\mathrm{T}})$ is the stress tensor, p_i is the pressure, ρ_i is the density, μ_i is the viscosity and $\mathbf{g}$ is the gravitational acceleration.

In the far-field, we assume that

$$\mathbf{u} = \mathbf{u}_\infty \text{ on } \partial\Omega. \tag{3}$$

Across the interface Σ, the velocity is continuous

$$0 = [\mathbf{u}]_\Sigma \equiv \left(\mathbf{u}|_{\Sigma,2} - \mathbf{u}|_{\Sigma,1}\right) \tag{4}$$

and the Laplace–Young jump condition holds [28]

$$[\mathbf{Tn}]_\Sigma = \sigma\kappa\mathbf{n} - \nabla_{\mathrm{s}}\sigma, \tag{5}$$

where σ is the surface tension coefficient, $\mathbf{n}$ is the normal vector to Γ directed towards fluid 2, $\kappa = \nabla \cdot \mathbf{n}$ is the curvature of Γ (positive for spherical/circular interface) and $\nabla_{\mathrm{s}} = (I - \mathbf{n} \otimes \mathbf{n})\nabla$ is the surface gradient. The first term on the right-hand side of Eq. (5) is the capillary force and the second is the Marangoni force.

When surfactants are present, the Langmuir equation of state (EOS) [45] is often used to describe the relation between the surfactant concentration f and the surface tension σ

$$\sigma(f) = \sigma_0 + RTf_\infty \log(1 - f/f_\infty), \tag{6}$$

where σ_0 is the surface tension for a clean interface ($f = 0$), f_∞ is the surfactant concentration at maximum packing, R is the ideal gas constant and T is the temperature.

When the actual surfactant concentration $f \ll f_\infty$, then the following linear approximation of Eq. (6) can be used:

$$\sigma(f) = \sigma_0 - RTf. \tag{7}$$

Insoluble surfactants are convected and diffused along the interface. There is no transfer from/to the bulk either to/from the interface and the total surfactant mass

$$M = \int_\Sigma f \, \mathrm{d}\Sigma = \int_\Omega f\delta_\Sigma \, \mathrm{d}\Omega, \tag{8}$$

where δ_Σ is the surface delta function, is conserved in time. The local form of the conservation of surfactant mass is [21]

$$f_{\mathrm{t}} + \mathbf{u} \cdot \nabla f - \mathbf{n} \cdot (\nabla\mathbf{un})f = D_{\mathrm{s}}\nabla_{\mathrm{s}}^2 f, \tag{9}$$

where D_{s} is the surfactant diffusivity. See also [54,61,62] for other forms of Eq. (9).

2.2. The non-dimensionalization and the Stokes system

In this paper, for simplicity, we assume that the two fluids (e.g., drop and matrix) are density- and viscosity-matched: $\rho_1 = \rho_2 = \rho$ and $\mu_1 = \mu_2 = \mu$. We also assume that the far-field flow velocity is a simple shear: $\mathbf{u}_\infty = \dot{\gamma}y\mathbf{e}_y$, where $\mathbf{e}_y$ is the coordinate vector in the y-direction and $\dot{\gamma}$ is the shear rate. To make the problem dimensionless, we follow [21] and use the characteristic quantities: the radius of a drop a for length, the inverse shear rate $\dot{\gamma}^{-1}$ for time, the product $a\dot{\gamma}$ for velocity, the average surfactant concentration $f_{\mathrm{e}} = 1/|\Sigma|\int_\Sigma f \, \mathrm{d}\Sigma$ for f and the corresponding equilibrium surface tension $\sigma_{\mathrm{e}} = \sigma(f_{\mathrm{e}})$ for σ. By using the equilibrium surface tension, rather than the clean surface tension, we scale out the effect of the uniform lowering of surface tension that would occur if the surfactant distribution were constant. Thus, by using this non-dimensionalization, we emphasize the effect of non-uniform surfactant distribution.

The relevant dimensionless parameters are the Reynolds number Re, the Capillary number Ca, the surface Peclet number Pe, the surfactant elasticity E and coverage x

$$Re = \frac{\rho a^2 \dot{\gamma}}{\mu}, \quad Ca = \frac{\mu a \dot{\gamma}}{\sigma_{\mathrm{e}}}, \quad Pe = \frac{a^2 \dot{\gamma}}{D_{\mathrm{s}}}, \quad E = \frac{RTf_{\infty}}{\sigma_0}, \quad x = \frac{f_{\mathrm{e}}}{f_{\infty}}. \tag{10}$$

For simplicity, in this paper we focus on the case in which the $Re = 0$ and the inertial terms on the left-hand side of Eq. (1) may be dropped. The resulting Stokes system is

$$\Delta \mathbf{u}_i = \nabla p_i, \tag{11}$$

$$\nabla \cdot \mathbf{u}_i = 0 \tag{12}$$

in Ω_i together with boundary conditions

$$0 = [\mathbf{u}]_{\Sigma},$$

$$-[p]_{\Sigma}\mathbf{n} + [(\nabla \mathbf{u} + \nabla \mathbf{u}^{\mathrm{T}}) \cdot \mathbf{n}]_{\Sigma} = \frac{1}{Ca}(\sigma\kappa\mathbf{n} - \nabla_{\mathrm{s}}\sigma)$$

and σ is the non-dimensional surface tension given below in Eq. (16). The Stokes equations may be written as a system of Poisson equations for the velocity and pressure [32]. The first is the Laplace equation for the pressure which is obtained by taking the divergence of Eq. (11) and deriving the appropriate boundary conditions. The result is [32]

$$\nabla^2 p_i = 0 \text{ in } \Omega_i \tag{13}$$

with jump boundary conditions on Σ

$$[p]_{\Sigma} = -\frac{1}{Ca}\sigma\kappa, \quad \left[\frac{\partial p}{\partial n}\right]_{\Sigma} = \frac{1}{Ca}\nabla_{\mathrm{s}}^2\sigma, \tag{14}$$

and Neumann boundary conditions on $\partial\Omega$

$$\frac{\partial p}{\partial n} = \nabla^2 \mathbf{u} \cdot \mathbf{n} \text{ on } \partial\Omega. \tag{15}$$

Note that the non-dimensional surface tension σ in Eq. (14) is derived from either Eq. (6) or (7) and is given by

$$\sigma(f) = \frac{1 + E\ln(1 - xf)}{1 + E\ln(1 - x)} \quad \text{or} \quad \sigma(f) = \frac{1 - Exf}{1 - Ex}, \tag{16}$$

respectively.

Once the pressure is determined, the velocity is obtained by solving the Poisson system [32]

$$\nabla^2 \mathbf{u}_i = \nabla p_i, \quad \text{in } \Omega_{\mathrm{i}} \tag{17}$$

together with the jump boundary conditions

$$[\mathbf{u}]_{\Sigma} = 0, \quad \left[\frac{\partial \mathbf{u}}{\partial n}\right]_{\Sigma} = \frac{1}{Ca}\nabla_{\mathrm{s}}\sigma, \tag{18}$$

and the far-field Dirichlet boundary condition

$$\mathbf{u} = y\mathbf{e}_y \text{ on } \partial\Omega. \tag{19}$$

The Poisson equations for pressure and velocity are exactly in a form appropriate for use with the immersed interface method (IIM). The IIM is described briefly in Section 3.1. The extension of this approach to flows with non-zero Reynolds numbers (but matched viscosities and densities) is straightforward using the techniques described in [27,30,37] for the IIM. The extension to flows with variable viscosity has also been recently developed [36].

Finally, the non-dimensional form of the surfactant equation is identical to Eq. (9) with D_s replaced by $1/Pe$.

2.3. Interface representation

To represent the interface, it is convenient to use the level-set approach. The level-set method was introduced by Osher and Sethian [44] and has become an increasingly popular method for simulating multifluid flows (e.g., see the recent reviews [43,51]).

Let $\phi(\mathbf{x}, t)$ be a scalar function whose zero level set $\{\mathbf{x}: \phi(\mathbf{x}, t) = 0\}$ represents the interface Σ. For example, we may set $\phi(\mathbf{x}, t)$ to be the signed distance from the point $\mathbf{x}$ to Σ at time t. Since the interface moves with the fluid, we may take

$$\frac{\partial \phi}{\partial t} + \mathbf{u} \cdot \nabla \phi = 0. \tag{20}$$

That is, all level surfaces of ϕ move with the fluid. In practice, this causes spatial compression/expansion of the level surfaces which is detrimental for accurate interface resolution (e.g. [57,59]). To avoid this, the level-set function is re-initialized after each time step to be a signed distance function locally near the interface [57,59]. This is performed by solving the following Hamilton–Jacobian equation to steady-state

$$\begin{cases} \phi_\tau + S(\phi_0)(|\nabla\phi| - 1) = 0, \\ \phi(\mathbf{x}, 0) = \phi_0(\mathbf{x}), \end{cases} \tag{21}$$

where ϕ_0 is the level-set function before the re-initialization, and the τ is the pseudo-time and $S(x)$ is the sign function of x defined as

$$S(x) = \begin{cases} -1 & \text{if } x < 0, \\ 0 & \text{if } x = 0, \\ 1 & \text{if } x > 0. \end{cases} \tag{22}$$

In practice, the re-initialization is performed at every time step.

One of advantages of the level-set method is that geometrical quantities can be easily computed. Assume that the set of $\mathbf{x}$ such that $\phi(\mathbf{x}, t) < 0$ is contained in Ω_1, then the outward normal, curvature and surface delta function of the interface Σ are

$$\mathbf{n} = \frac{\nabla\phi}{|\nabla\phi|}, \quad \kappa = \nabla \cdot \left(\frac{\nabla\phi}{|\nabla\phi|}\right), \quad \delta_\Sigma = \delta(\phi)|\nabla\phi|, \tag{23}$$

where $\delta(x) = \mathrm{d}S/\mathrm{d}x$ is the usual one-dimensional delta function.

3. The numerical method

3.1. The immersed interface method

The Stokes equations are solved using the IIM. Let $\{\mathbf{x}_{i,j} = (x_i, y_j): 0 \leqslant i \leqslant N, 0 \leqslant j \leqslant N_1\}$ denote a uniform Cartesian mesh. Let h be the step size in both x- and y-directions. The resulting scheme is an approximate projection method in that the velocity field is not exactly divergence-free on the discrete level.

A grid point $\mathbf{x}_{i,j}$ is called irregular if the level-set function ϕ changes the sign from $\mathbf{x}_{i,j}$ to its four neighbors $\mathbf{x}_{i+1,j}$, $\mathbf{x}_{i-1,j}$, $\mathbf{x}_{i,j+1}$, and $\mathbf{x}_{i,j-1}$, otherwise it is called regular. At an irregular grid point, conventional (central) finite difference scheme may not be accurate since the stencil contains grid points from both sides of the interface and the solution and/or its derivatives may be discontinuous across the interface.

The idea of the IIM is to design truly second-order accurate finite difference schemes at all points- both regular and irregular. The schemes explicitly incorporate the jump conditions while maintaining standard forms of the discrete system so that fast solvers can be used. We refer the readers to [19,31,34] for the detailed construction of such finite difference schemes at irregular grid points. Here, we highlight the main idea by illustrating the scheme applied to a Poisson equation

$$\Delta w = f$$

with jump conditions

$$[w]_\Sigma \quad \text{and} \quad [\partial w/\partial \mathbf{n}]_\Sigma \text{ given.}$$

Using the IIM, the finite difference scheme, applied to the above equation, is simply the following:

$$\frac{w(x_{i+1},y_j) + w(x_{i-1},y_j) + w(x_i,y_{j+1}) + w(x_i,y_{j-1}) - 4w(x_i,y_j)}{h^2} = f(x_i,y_j) + C_{i,j} + E_{i,j}, \tag{24}$$

where $E_{i,j}$ is $O(h^2)$ at regular grid points, and is $O(h)$ at irregular grid points, the correction term $C_{i,j}$ is zero at regular grid points but is non-zero at irregular grid points and depends on the jumps $[w]_\Sigma$ and $[\partial w/\partial \mathbf{n}]_\Sigma$. Note that a fast Poisson solver such as the FFT can be used for solving the discrete system (24). The derivation of the correction terms $C_{i,j}$ involves the following:

- Identify the control points $\mathbf{x}^* = (x^*, y^*)^{\mathrm{T}}$ associated with each irregular point $\mathbf{x} = (x_i, y_j)^{\mathrm{T}}$. We take $\mathbf{x}^* = (x^*, y^*)^{\mathrm{T}}$ to be the orthogonal projection of $\mathbf{x} = (x_i, y_j)^{\mathrm{T}}$ on the interface (e.g. [19]).
- Use the Taylor expansions of $w(x_i, y_j)$, $w(x_{i+1}, y_j)$, $w(x_{i-1}, y_j)$, $w(x_i, y_{j+1})$, and $w(x_i, y_{j-1})$ at the control points $\mathbf{x}^*$ up to second-order derivatives from the each side of the interface.
- Use the interface relations to represent all the quantities (up to second-order derivatives) after the Taylor expansions from one particular side in terms of those from the other.
- Solve for C_{ij} in (24) after the procedures above and ignoring higher-order terms to get the correction term.

The interface relations are derived from the two given jump conditions, their surface derivatives, and the differential equations. The interface relations and the derivation can be found in [31,34].

Remark. For an elliptic equation with discontinuous coefficients, additional grid points $(x_{i+i_0},\ y_{j+j_0})^{\mathrm{T}}$, with $i_0,\ j_0 = -1$ or 1 are required to construct second-order accurate finite difference schemes at irregular grid points, see [35].

The technique described above is used for solving the scalar pressure and the vector velocity Poisson equations. However, since p is discontinuous across the interface, care needs to be taken to evaluate the right-hand side, ∇p, of the velocity Poisson equations (17).

The approximation of p_x is as follows (p_y is treated similarly). At regular grid points we use the standard central finite difference scheme. If an irregular grid point (x_i, y_j) is on the same side of the interface as (x_{i+1}, y_j) or (x_{i-1}, y_j), we use the forward or the backward finite difference scheme. If (x_i, y_j) is in one side of the interface, but both (x_{i+1}, y_j) and (x_{i-1}, y_j) are on the other side, neither central finite difference scheme, nor the one-sided difference scheme is suitable because p is not continuous in $[x_{i-1}, x_i]$ or $[x_i, x_{i+1}]$. In this case, the following finite difference scheme is used:

$$(p_x^{\pm})_{ij} = \frac{p_{ij} - p_{lj} \mp [p] \mp [p_x](x_l - x^*) \mp [p_y](y_j - y*)}{x_i - x_l}, \tag{25}$$

where $l = i + 1$ or $l = i - 1$ is chosen such that $|x_l - x^*| = \min\{|x_{i-1} - x^*|, |x_{i+1} - x^*|\}$, and the '+' sign is taken if $\phi(x_i, y_j) > 0$, otherwise '−' sign is taken. In Eq. (25), (x^*, y^*) is the control point associated with (x_i, y_j) on the interface. The derivation of the jumps $[p_x]$, $[p_y]$ and the error analysis can be found in [32,34].

3.2. Discretization of the interface jump conditions

To evaluate the jump conditions (14) and (18) on the discrete level, we use the following methodology. First, as discussed below, the surfactant concentration is extended and evolved in small tubes containing the interface. Accordingly, the surface tension is also defined in this region (see Sections 3.3 and 3.5). Standard centered difference schemes are then used to discretize κ, $\nabla_s\sigma$ and $\nabla_s^2\sigma$ (using (28)) at grid points in a smaller tube containing the interface. These quantities are then interpolated at the control points of the irregular grid points using cubic interpolation.

3.3. The evolution of the surfactant concentration and its extension

As mentioned above, it is useful to extend the surfactant concentration f off the interface Σ into a small neighborhood around Σ. This has the advantage that conventional difference/element methods can be used for solving the surfactant transport equation [62] and for evaluating the interface jump conditions.

To extend f off the interface, we solve the following Hamilton–Jacobian equation:

$$\begin{cases} f_\tau + S(\phi)\mathbf{n} \cdot \nabla f = 0, \\ f(\mathbf{x}, 0) = f_0(\mathbf{x}), \end{cases} \tag{26}$$

where as before $S(x)$ is the sign function of x, see Eq. (22). The effect of this evolution equation is to leave the value of f at the interface unchanged (since the sign function is zero at $\phi(\mathbf{x}) = 0$) while propagating the values of f in the normal direction away from the interface with speed one. This extension scheme first proposed in [65] is a standard method for extending quantities off interfaces in level-set method [1,6]. In practice a smoothed sign function is used

$$\widetilde{S}(\phi) = \frac{\phi}{\sqrt{\phi^2 + h^2}}, \tag{27}$$

where h is the spatial step size.

An upwind third-order WENO method and a third-order TVD Runge-Kutta method are used for the spatial and temporal discretizations, respectively, of Eq. (26). At every time step (in t), the extension is performed for a few pseudo-time (τ) steps since we only need to extend f in a neighborhood of the interface. Further details can be found in [62].

To solve the surfactant transport equation (9), we use a semi-implicit scheme developed by Xu and Zhao [62]. In this scheme, the surface Laplacian is rewritten as

$$\nabla_s^2 f = \nabla^2 f - \frac{\partial^2 f}{\partial \mathbf{n}^2} - \kappa \frac{\partial f}{\partial \mathbf{n}} \tag{28}$$

and correspondingly, Eq. (9) is rewritten as

$$f_t + \mathbf{u} \cdot \nabla f - \mathbf{n} \cdot (\nabla \mathbf{u}\mathbf{n}) f = \frac{1}{Pe}\left(\nabla^2 f - \frac{\partial^2 f}{\partial \mathbf{n}^2} - \kappa \frac{\partial f}{\partial \mathbf{n}}\right). \tag{29}$$

This makes it apparent that an explicit time marching method for Eq. (29) requires that the time step $\Delta t \sim h^2$ for stability. To remove this restriction, the leading-order term $\nabla^2 f$ can be discretized implicitly while all other terms can be treated explicitly [62]. To achieve second-order accuracy in time, a semi-implicit Crank–Nicholson scheme is used

$$\frac{f^{m+1}-f^m}{\Delta t} = \frac{1}{Pe}\frac{\nabla^2 f^{m+1}+\nabla^2 f^m}{2} + \frac{3}{2}\left[-\frac{1}{Pe}\left(\kappa\frac{\partial f}{\partial \mathbf{n}}+\frac{\partial^2 f}{\partial \mathbf{n}^2}\right) - \mathbf{u}\cdot\nabla f + \mathbf{n}\cdot(\nabla\mathbf{un})f\right]^m - \frac{1}{2}\left[-\frac{1}{Pe}\left(\kappa\frac{\partial f}{\partial \mathbf{n}}+\frac{\partial^2 f}{\partial \mathbf{n}^2}\right) - \mathbf{u}\cdot\nabla f + \mathbf{n}\cdot(\nabla\mathbf{un})f\right]^{m-1}. \tag{30}$$

In the spatial discretization of Eq. (30), central difference schemes are used for all terms except for the advection term $\mathbf{u}\cdot\nabla f$ where an upwinding third-order WENO scheme is used (e.g. [23,24]). We refer the reader to [62] for the stability analysis of the semi-implicit Crank-Nicholson scheme.

The resulting linear system at each time step is similar to that from a heat equation and can be solved easily since the coefficient matrix is symmetric and positive definite.

3.4. Advection of the level-set function

To evolve the level-set function from (20) with a given velocity field $\mathbf{u}$, we use an upwinding third-order WENO method for the spatial discretization and a third-order TVD Runge–Kutta method (e.g. [53]) for the time discretization. It is necessary to use high-order schemes to achieve accurate approximations of the normal vector and the interface curvature.

At every time step, the level-set is reinitialized by solving equation (21) using third-order WENO and the third-order TVD Runge–Kutta method. The sign function is smoothed as in the extension algorithm.

3.5. Local level-set method

To efficiently update the level-set function and the surfactant concentration f, we use the local level-set method [46]. Accordingly, we construct four tubes $T_i = \{x\colon |\phi(x)| \leqslant \gamma_i\}$, $i = 1, \ldots, 4$, around the interface in which PDEs for the level-set function and surfactant concentration are solved, respectively (see [62]). The widths γ_i's are usually a few grid sizes. The exact choice depends on the stencils of the spatial discretization for the level-set convection equation, the jump conditions and the evolution of surfactant concentration. For our discretization choices, we choose tube widths as follows. Let h be the space step size, we take $\gamma_1 = 9h$, $\gamma_2 = 8h$, $\gamma_3 = 5h$, $\gamma_4 = 12h$. The surfactant concentration is extended into the region T_1, the surfactant transport equation is solved in region T_2, the surface tension σ is calculated in region T_2, $\nabla_s\sigma$, $\nabla_s^2\sigma$ and the jump conditions used in IIM are calculated in region T_3, the level-set convection equation is solved in region T_1 and reinitialization is performed in region T_4.

3.6. Enforcing area and surfactant conservation

One of the drawbacks of the level-set method is that area (mass of component) is not exactly conserved by the flow. In addition, surfactant mass is not exactly conserved by our algorithm either. Typically, small errors in each step of the algorithm are incurred at every time step and after long times these errors may accumulate and lead to inaccurate results.

There have been a number of efforts to improve area conservation for a clean surface. For example, a constrained re-initialization method is proposed in [57] to improve the area conservation. However, we have found that the method does not work well for our problem. In [58], the level-set method and the volume of fluid method were coupled together to achieve conservation, and in [12] a hybrid particle level-set approach was proposed to more accurately conserve mass.

In our numerical simulations, we have noticed that the discrete velocity field obtained from the IIM is typically not exactly divergence free. This is because the discrete divergence of the discrete gradient operator does not give the discrete Laplacian operator that is used in the IIM. This is especially true in the presence of interface jump conditions. As such, the IIM falls into the category of approximate projection methods where the divergence of the velocity is not zero on the discrete level but tends to zero as the grid size vanishes (at a second-order rate). Our results indicate that this is the main factor in the loss of area conservation. Therefore, to enforce area conservation, a small correction is added to the normal velocity of each moving interface. This is an approach frequently used in boundary integral simulations (e.g., see [8]). Let $\tilde{\mathbf{u}}_h$ be the discrete velocity obtained from the IIM. Accordingly, we determine a small correction α such that

$$\int_{\Omega} \nabla \cdot (\tilde{\mathbf{u}}_h + \alpha \nabla\phi/|\nabla\phi|)\, \mathrm{d}\Omega = \int_{\Sigma} (\tilde{\mathbf{u}}_h + \alpha\mathbf{n}) \cdot \mathbf{n}\, \mathrm{d}s = 0,$$

where Ω is the region enclosed by the interface Σ. This yields the explicit expression

$$\alpha = -\frac{\int_{\Sigma} \tilde{\mathbf{u}}_h \cdot \mathbf{n}\, \mathrm{d}s}{\int_{\Sigma} \mathrm{d}s} = -\frac{\int \tilde{\mathbf{u}}_h \cdot \mathbf{n}\delta_{\Sigma}(\phi)\, \mathrm{d}\mathbf{x}}{\int \delta_{\Sigma}(\phi)\, \mathrm{d}\mathbf{x}}. \tag{31}$$

The (modified) velocity $\mathbf{u}_h = \tilde{\mathbf{u}}_h + \alpha\mathbf{n}$, with $\mathbf{n}$ extended off the interface in the natural way $\mathbf{n} = \nabla\phi/|\nabla\phi|$, is then used to advect the level-set function and the surfactant concentration. The modification above ensures that the total mass flux across the interface is zero and is found to result in dramatically reduced mass loss overall.

Although the (modified) velocity $\mathbf{u}_h$ is also used in the evolution of the surfactant concentration (30) and does improve the conservation of surfactant mass, we find, however, that at long times there can still be significant loss of surfactant due to numerical diffusion (and leakage off the interface). We therefore introduce an additional correction step to enforce surfactant conservation. The simplest way to enforce this correction is to multiply the surfactant concentration by a constant factor to ensure that total surfactant mass is conserved. Let $\tilde{f}_h$ be the solution of the discrete surfactant equation (30) and let f_0, ϕ_0 and Σ_0 be the initial surfactant concentration, level-set function and interface, respectively. Then, we choose β such that

$$\int_{\Sigma} \beta\tilde{f}_h\, \mathrm{d}\Sigma = \int_{\Sigma_0} f_0\, \mathrm{d}\Sigma_0, \tag{32}$$

which yields

$$\beta = \frac{\int_{\Sigma_0} f_0\, \mathrm{d}\Sigma_0}{\int_{\Sigma} \tilde{f}_h\, \mathrm{d}\Sigma} = \frac{\int_{\Omega} f_0 \delta_{\Sigma_0}\, \mathrm{d}\mathbf{x}}{\int_{\Omega} \tilde{f}_h \delta_{\Sigma}\, \mathrm{d}\mathbf{x}}. \tag{33}$$

The surfactant concentration is then reset to be $f_h = \beta\tilde{f}_h$. We refer the reader to [62] for numerical approximations of the delta function in the above integrals (recall from Eq. (23) that $\delta_{\Sigma} = \delta(\phi)|\nabla\phi|$). The smoothing length of the delta function is less than the tube widths where the equations are solved. The integrals themselves are approximated by the trapezoid rule.

Finally, we note that other, more sophisticated area and surfactant concentration corrections can be derived that take into account the interface curvature and the surfactant concentration gradients. Nevertheless, we found it sufficient to use the simpler corrections described above.

4. Numerical results

In this section, we present 2D simulations illustrating the effect of surfactant on the evolution of a single drop in shear flow, drop–drop interactions among two drops as well as interactions among multiple drops.

4.1. Single drop

Consider an initially circular drop of radius 1 placed in a computational domain $\Omega = [-4, 4] \times [-2, 2]$. The initial surfactant distribution $f = 1$ on the surface of the drop. A steady shear flow is applied, at times $t > 0$. When the Capillary number is small, e.g., $Ca = 0.05$, we find that the drop deforms only slightly and evolves fairly quickly to a steady-state (not shown) consistent with previous studies (e.g. [55]). Here, we focus on the more interesting case with Capillary number $Ca = 0.7$ where the deformation is large. A uniform Cartesian grid is used with $h_x = h_y = h = 0.005$. The time step is $\Delta t = h/8$.

4.1.1. Linear equation of state

In Fig. 1a, the evolution of the drop under steady shear flow is shown at times $t = 0$, 3, 6 and 9 using the linear equation of state (16) with $E = 0.2$ and surfactant coverages $x = 0$ (dotted), $x = 0.1$ (dash-dot) and $x = 0.3$ (solid). The Peclet number is $Pe = 10$. As expected, the drop deformation is an increasing function of surfactant coverage.

In Fig. 1b, the corresponding surfactant concentration (left column) and surface tension (right column) are plotted versus arclength s for the cases $x = 0.1$ (dash-dot) and $x = 0.3$ (solid). In these plots, time increases from top to bottom. To make this plot, the interface is reconstructed by projecting the irregular grid points onto interface control points. A piecewise linear representation of the interface is used to calculate arclength. The starting point $s = 0$ corresponds to the control point closest to the positive x-axis and s increases in the counterclockwise direction. The surfactant concentration and surface tension on the interface are obtained by cubic interpolation at the control points.

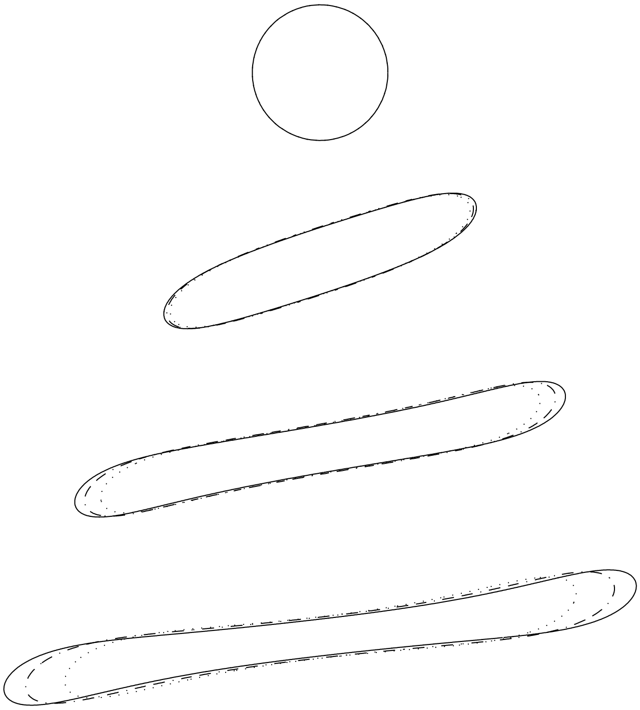

Fig. 1a. Effect of linear EOS and coverage x on drop shape at times $t = 0$, 3, 6 and 9. $Ca = 0.7$, $E = 0.2$ and $Pe = 10$. Solid, $x = 0.3$; dash-dot, $x = 0.1$; dotted, $x = 0$ (no surfactant).

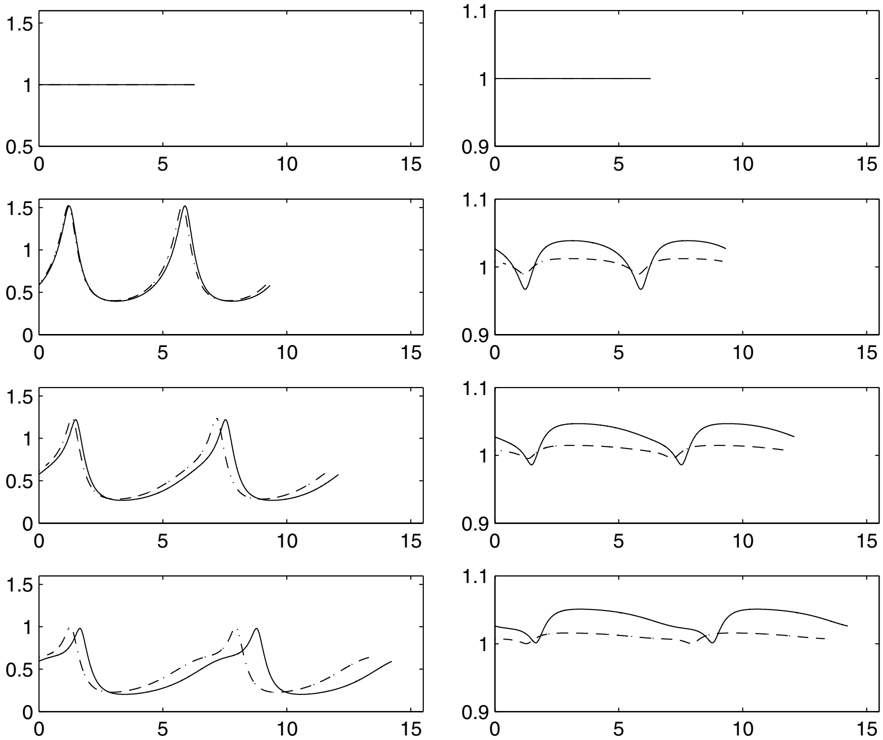

Fig. 1b. Effect of linear EOS and coverage x on surfactant concentration (left column) and surface tension (right column). Notation, times and parameters as in Fig. 1a.

As seen in the figure, surfactant is swept to the drop tips by the flow. The resulting surface tension is non-uniform with the smallest surface tension occurring at the drop tips. Increasing the initial surfactant coverage has the primary effect of increasing the variation of the surface tension along the interface. The distribution of surfactant is only slightly affected by the surfactant coverage; the surfactant distributions are shifted slightly because they are plotted with respect to the arclength along the drop.

In Fig. 1c, the corresponding capillary (left column) and the Marangoni forces (right column) are plotted as a function of arclength for the different cases. The Capillary force is defined as $-\sigma\kappa/Ca$ and the Marangoni force is $\nabla_s\sigma \cdot \mathbf{s}/Ca$ ($\mathbf{s}$ is the tangential direction) which are calculated on the Cartesian mesh and obtained by cubic interpolation at the control points.

The capillary force is largest in magnitude at the drop tips due to the high curvature. At the tips, the force is negative indicating the tendency to drive the drop-tips inward and thus the drop shape to become more circular. The magnitude of the capillary force is largely independent of the surfactant coverage; the magnitude at the drop tips is slightly larger for the larger surfactant coverage because the corresponding drop-tip has a larger curvature.

At the drop tip, the Marangoni force is zero due to symmetry. Near the drop tips, the Marangoni force has positive and negative peaks that act to resist the surfactant redistribution and accumulation at the drop tip. The variation of the Marangoni force increases with increasing surfactant coverage. Nevertheless, near the drop-tip, the magnitude of the Marangoni force is more than two orders of magnitude smaller than the Capillary force for $x = 0.3$.

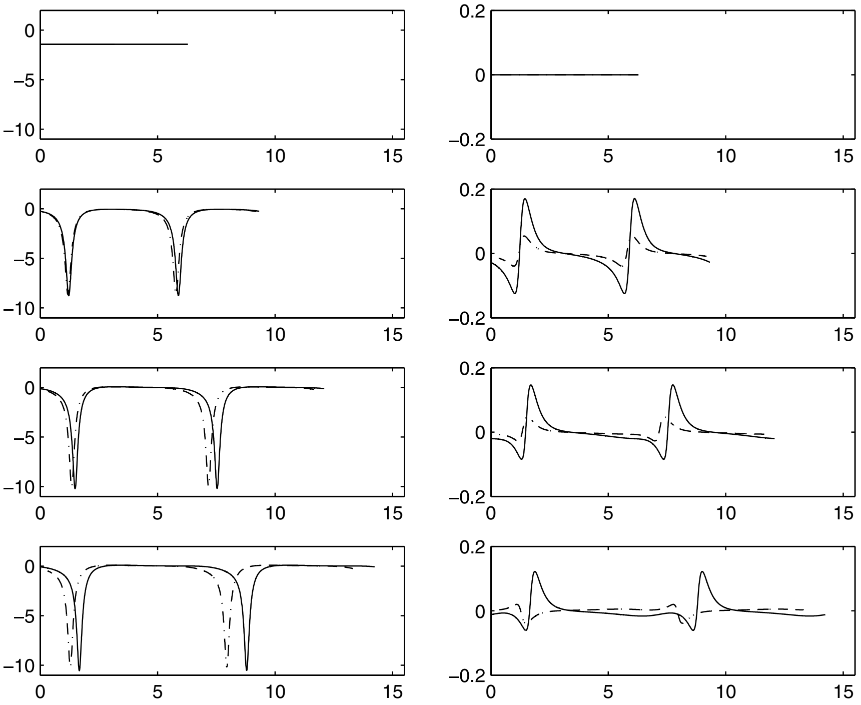

Fig. 1c. Effect of linear EOS and coverage x on Capillary force (left column) and Marangoni force (right column). Notation, times and parameters as in Fig. 1a.

Next, we examine the numerical errors associated with these calculations. In Fig. 1d, we present the relative errors in drop area (upper left) and surfactant mass (lower left) together with the area correction α (upper right) and surfactant mass correction β (lower right). The results are shown for the coverage $x = 0.1$; the results with $x = 0.3$ are similar. The errors in drop-area and surfactant mass are very small – the errors in area and surfactant mass are approximately 0.01% and 0.001%, respectively. This indicates that the area and surfactant mass correction algorithms are very effective. The actual values of α and $\beta - 1$ are approximately 10^{-3} and 10^{-5}, respectively.

To test the convergence of the algorithm, we perform a resolution study and focus on the maximum distance from the drop interface to the drop center. The maximum distance is plotted as a function of time for three resolutions ($x = 0.1$) in Fig. 1e(left). From these results, an order of convergence is estimated and is shown in Fig. 1e(right). After an initial transient, the order of convergence seems to settle between 3 and 4.

4.1.2. Nonlinear equation of state

In Fig. 2a, the evolution of the drop under steady shear flow is shown at times $t = 0$, 3, 6 and 9 using the linear (solid) and nonlinear (dashed) equations of state from Eq. (16) with $E = 0.2$ and $x = 0.3$. Consistent with previous work (e.g. [45,21]), the drop deformation is seen to increase when the nonlinear equation of state is used. The corresponding surfactant concentrations and surface tensions are shown in Fig. 2b. At early times ($t \approx 3.0$), the surface tension at the drop-tip is lower when the nonlinear equation of state is used. This results in the observed larger deformation. As seen in Fig. 2c(right), this also leads to a larger Marangoni force. The Capillary forces are roughly similar, see Fig. 2c(left), with the nonlinear case having a slightly larger force at the drop-tip due to the larger curvature at the drop-tip.

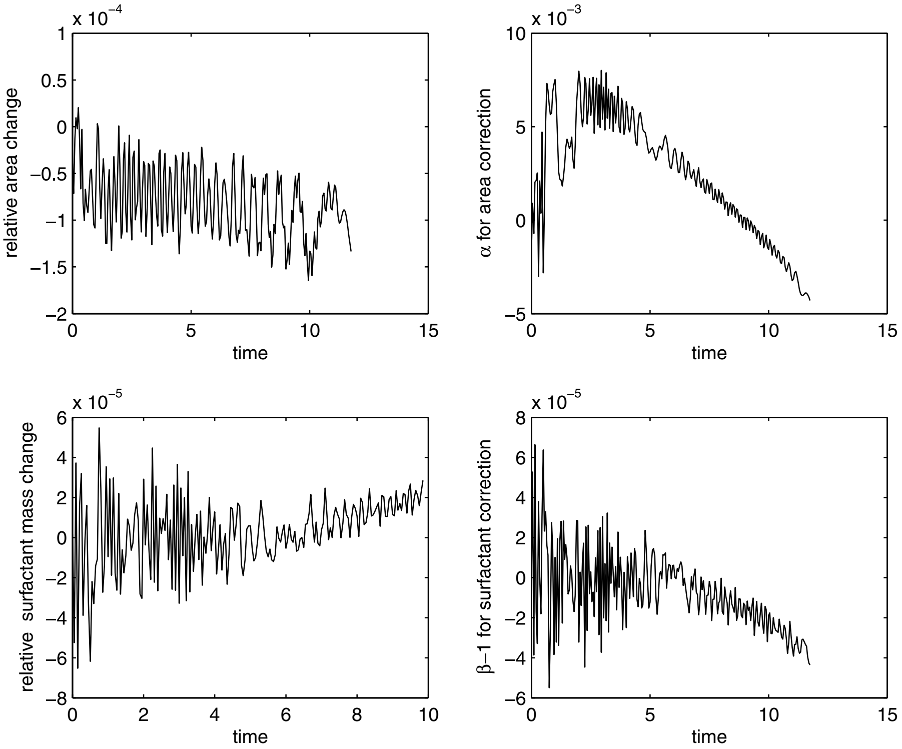

Fig. 1d. Relative errors for linear EOS with $x = 0.1$. All other parameters as in Fig. 1a. Upper left: drop area; lower left: surfactant mass; upper right: area correction α; lower right: surfactant mass correction β.

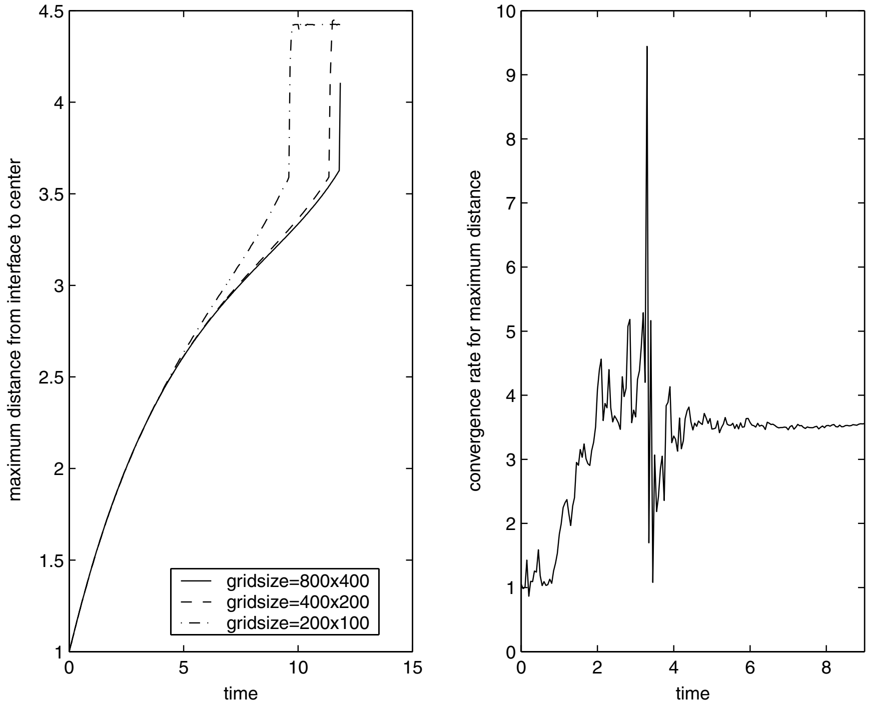

Fig. 1e. Convergence for the maximum distance from the drop-interface to the centroid using linear EOS with $x = 0.1$. Other parameters as in Fig. 1a. (Left) maximum distance; (right) order of convergence.

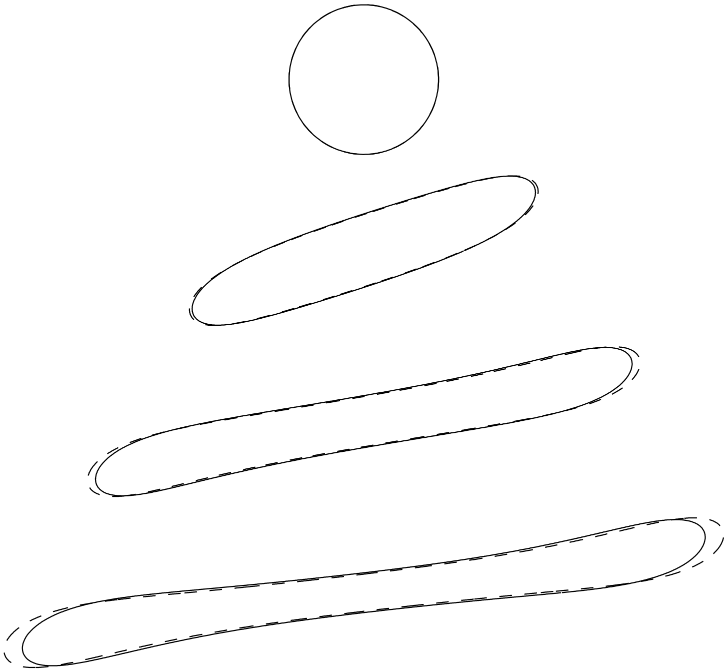

Fig. 2a. Evolution of drop shape with linear (solid) and nonlinear (dashed) EOS at times $t = 0$, 3, 6 and 9 with $Ca = 0.7$, $E = 0.2$ and $x = 0.3$.

4.2. Two drops

We next consider the effect of surfactant on drop–drop interactions in a steady shear flow with Capillary number $Ca = 0.5$. We consider two initially circular drops with radii equal to 1 and with centroids located at $(-1.7, 0.25)$ and $(1.7, -0.25)$. The computational domain is $[-7, 7]\times[-5, 5]$, the spatial grid size is $h_x = h_y = h = 0.01$ and the time step is $\Delta t = h/8$.

In Fig. 3a, the drop evolution is shown, at times $t = 0$, 2, 4, 6, 8 and 10, in the absence of surfactant $x = 0$ (dotted) and with surfactant (solid) where $E = 0.2$, $x = 0.3$ and $Pe = 10$. The surfactant concentration f is initially uniform and equal to 1. As the drops approach one another, they are deformed by the flow with the surfactant case being slightly more deformed. As the drops interact, they flatten and a dimple forms in the near contact region due to lubrication forces. As the drops pass by one another the trailing-edge drop-tips in the near contact region first flatten and then elongate due to local straining flows that develop as the drops separate. The separated drops with surfactant are more elongated and rotated than the surfactant-free drops. We note that errors (not shown) in the drop areas and the surfactant masses on each of the drops are less than 1% throughout the entire simulation.

In Fig. 3b, the corresponding (unmodified) velocity vectors relative to the applied shear flow, $\tilde{\mathbf{u}}_h - (y,\ 0)$, are shown for the drop with initial centroid located at $(-1.7, 0.25)$. From top to bottom the times are $t = 2$, 6 and 10. The left column corresponds to the case without surfactant. Near the interface at this resolution the modified velocity field is identical to the unmodified velocity shown in the figure; this is to be expected since the area/velocity correction parameter α is approximately 10^{-3}. The velocity fields with and without surfactant are qualitatively quite similar, however, there are quantitative differences that result in the enhanced rotation and stretching of the drop with surfactant. The differences are manifest in the structure and location of the two vortices off the drop as well as the velocity near the drop-tips and the drop-centers.

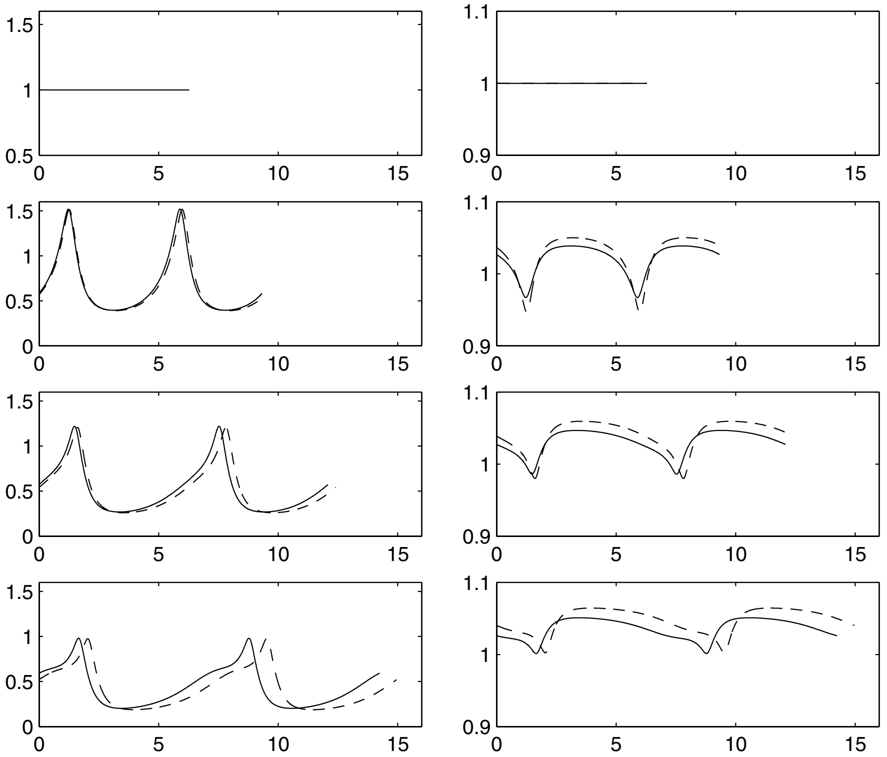

Fig. 2b. Evolution of surfactant concentration (left column) and surface tension (right column) from Fig. 2a.

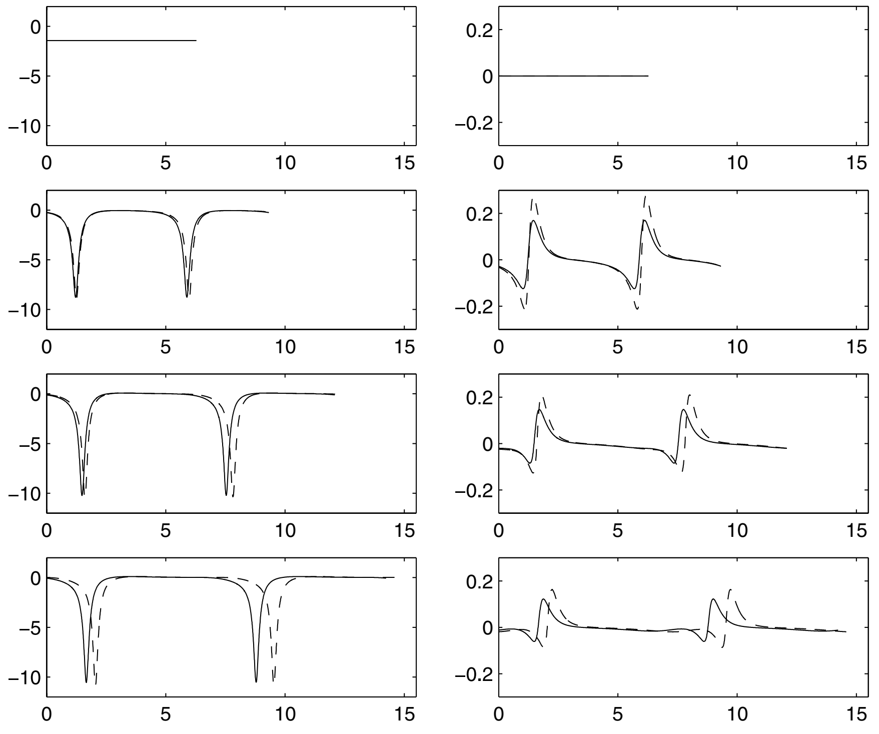

Fig. 2c. Evolution of Capillary force (left column) and Marangoni force (right column) from Fig. 2a.

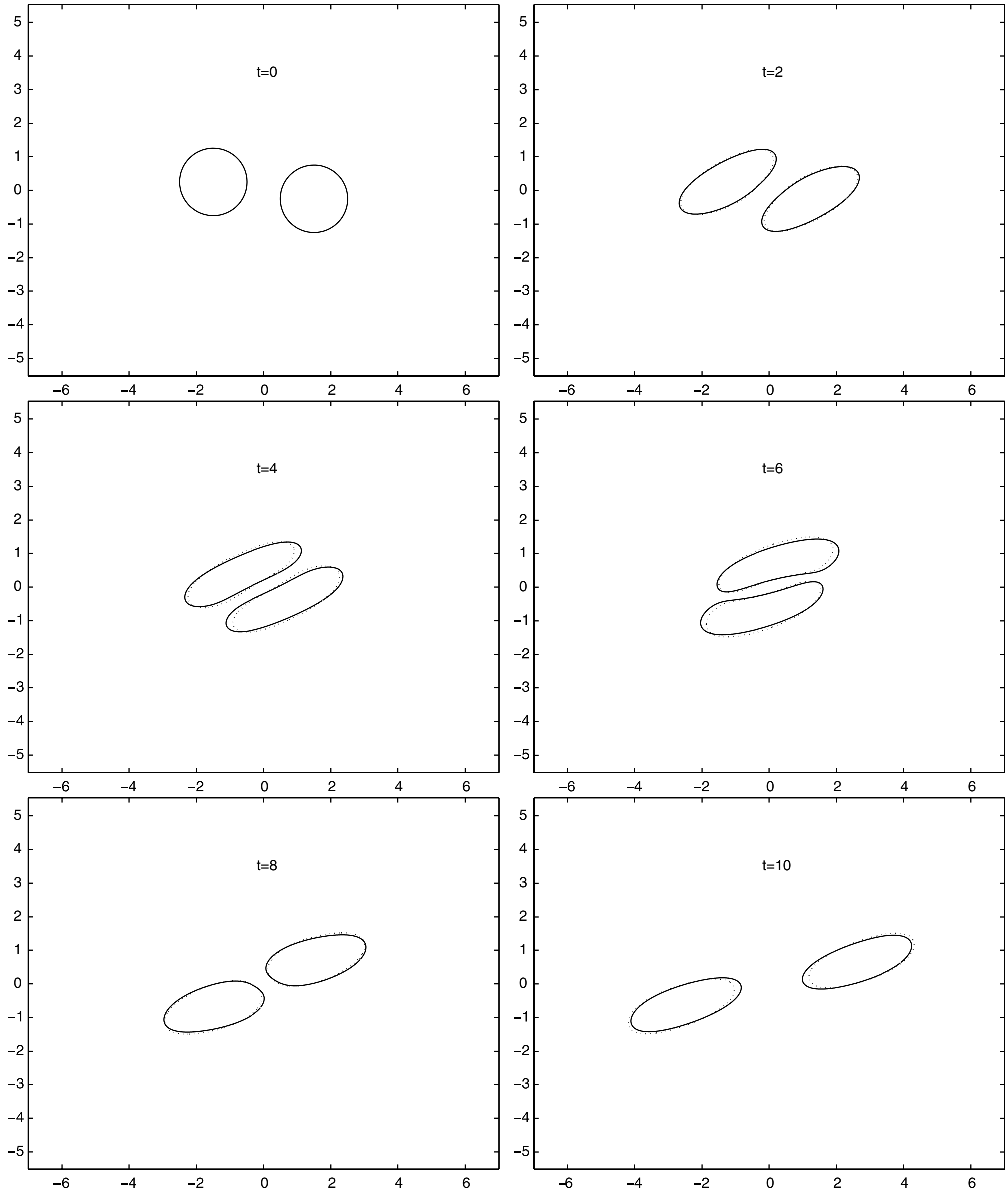

Fig. 3a. Morphologies of two drops in shear flow with $Ca = 0.5$, nonlinear EOS (solid) with $E = 0.2$, $x = 0.3$ and $Pe = 10$. Dotted: $x = 0$ (no surfactant). Times are $t = 0$, 2, 4, 6, 8 and 10.

The evolution of the surfactant concentrations on each drop are shown in Fig. 3c. The left column corresponds to the drop initially placed at (1.7, −0.25). During approach, the surfactant is swept to the drop tips and the distributions are similar to those observed in Section 4.1 for isolated drops. During interaction, surfactant is swept towards the part of the drops in near contact and the concentration near the leading-edge drop-tip is decreased. As the drops begin to separate, a large broad distribution of surfactant is present along the flattened drop-tip in the near contact region. Once the drops separate further, the distribution refocuses as surfactant is again swept towards the elongating drop-tips.

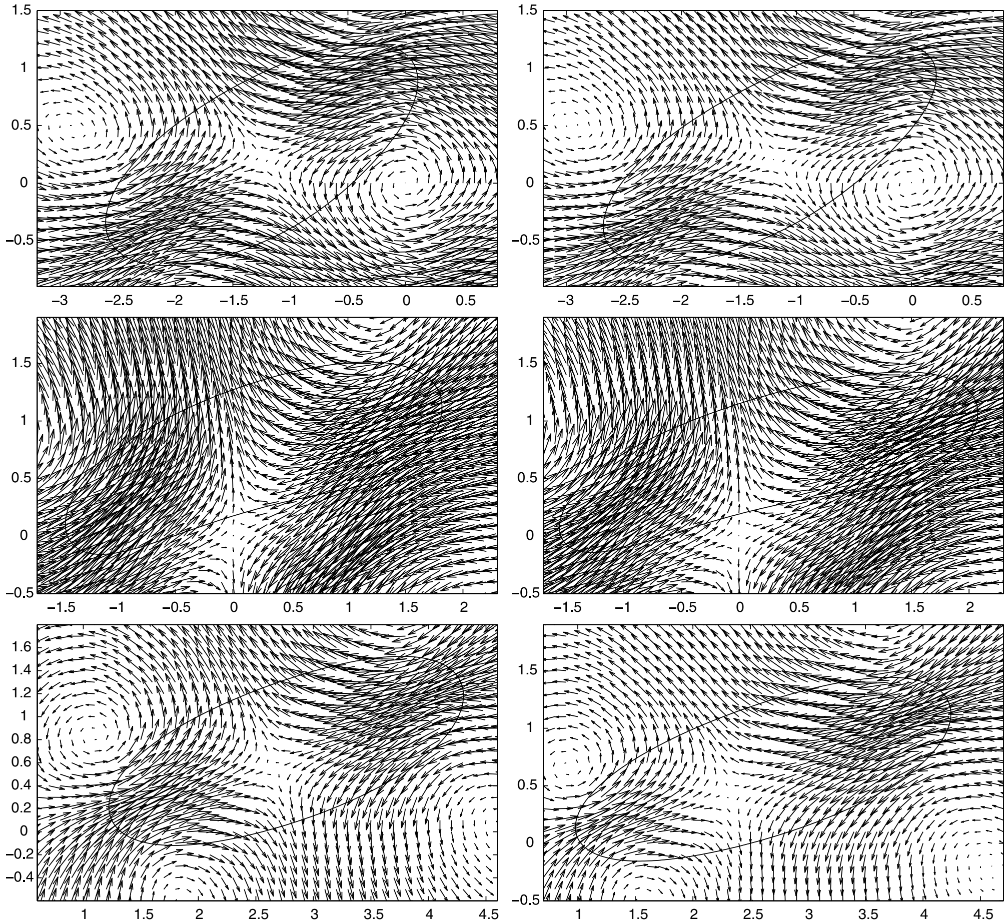

Fig. 3b. Velocity vectors and morphologies of the drops in Fig. 3a at times $t = 2$, 6 and 10 (top to bottom). (Left column) No surfactant; (right column) with surfactant.

In Fig. 3d, the minimum distance between the drops is plotted as a function of time for the clean (dotted) and surfactant covered (solid) drops. A blow-up of this graph is shown as an inset. During approach and interaction (times less than approximately 7.0) the presence of surfactant keeps the drops slightly farther apart than the clean case (see inset). However, as the drops begin to separate, the graphs cross and the drops with surfactant are closer to one another due to the fact that the trailing drop-tip is more elongated in the presence of surfactant. This has the following interesting consequence. Under conditions for which clean drops do not coalesce, surfactant laden drops will likely not coalesce upon approach since the drops are more deformed and hence there is more fluid to expel the fluid in the near contact region in order for the drops to coalesce compared to the clean case. However, the surfactant laden drops may coalesce upon separation since the trailing-edge drop tips are more elongated than in the clean case. This phenomena has been observed in experiments [29].

Another measure of the drop separation is the difference Δy in the y-coordinate of the drop centroids. In Fig. 3e, Δy is plotted with respect to the difference Δx in the x-coordinate of the centroids. Note that $\Delta y(t = 0) = 0.5$ and $\Delta x(t = 0) = -3.4$. As the drops approach (i.e., $\Delta x \leqslant -1.5$), the clean drops have smaller Δy. During interaction and separation, the opposite is true. The difference between the $\Delta y(t = 0)$ and

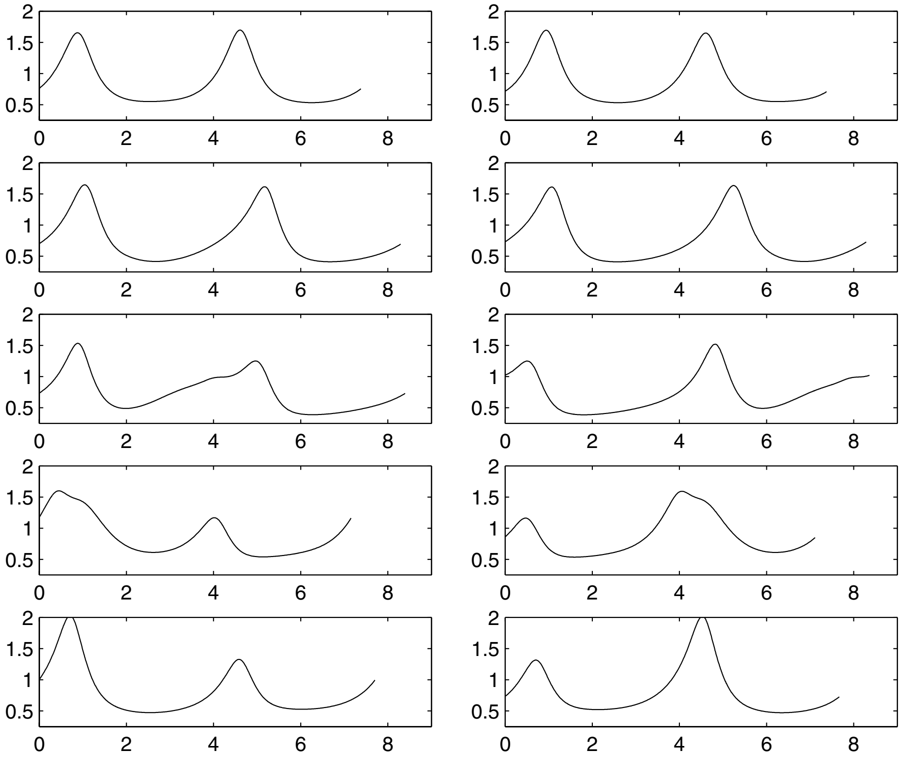

Fig. 3c. Surfactant concentrations on the drops as a function of arclength from Fig. 3a. (Left) Surfactant concentration from drop initially located at (1.7, −0.25). (Right) Surfactant concentration from drop initially located at (−1.7, 0.25). Times and parameters as in Fig. 3a.

$\Delta y(t_{\mathrm{final}})$ after interaction and separation is a measure of the so-called hydrodynamic diffusion [39]. That is, through hydrodynamic interactions, drops become more widely spaced than they were initially. This mimics the effects of diffusion. From this figure, the presence of surfactants is seen to decrease the hydrodynamic diffusion compared to the clean case. This is primarily because the surfactant laden drops are more rotated than the clean drops. Interestingly, this result suggests that dilute dispersions of drops with surfactant may be less spread out and may have smaller drop–drop distances than their clean counterparts. Further studies are being conducted to determine how this result depends on the Capillary number, the surfactant coverage and the initial separation distances.

4.3. Multiple drops

Lastly, we consider the effect of surfactant on systems with four interacting drops in a steady shear flow with Capillary number $Ca = 0.7$. Initially, the four drops are circular with radii equal to 1 and with centroids (−7.7, 1.05), (−1.7, 0.25), (1.7, −.25) and (7.7, −1.05). The computational domain is $[-9, 9]\times[-5, 5]$, the spatial grid size is $h_x = h_y = h = 0.01$ and the time step is $\Delta t = h/8$.

In Fig. 4a, the drop evolution is shown, at times $t = 0$–10.5 in increments of 1.5. in the absence of surfactant $x = 0$ (dotted) and with surfactant (solid) where $E = 0.2$, $x = 0.3$ and $Pe = 10$. The surfactant concentration f is initially uniform and equal to 1. As in the two-drop case, the four drops are deformed by the flow with the surfactant case being slightly more deformed. The two inner drops interact first leading to

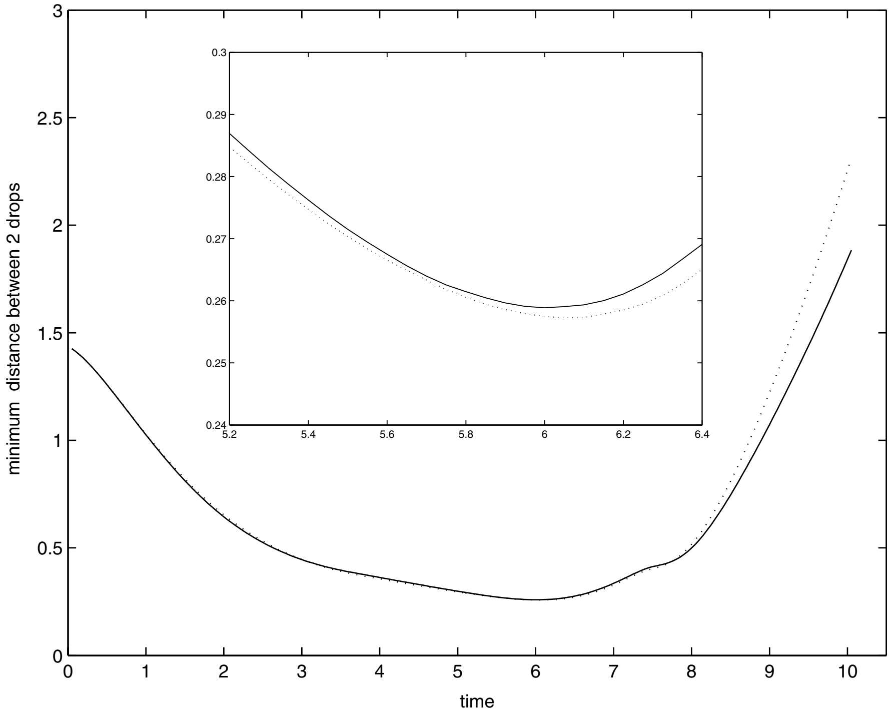

Fig. 3d. Minimum distance between the two drops in Fig. 3a. Notation as in that figure.

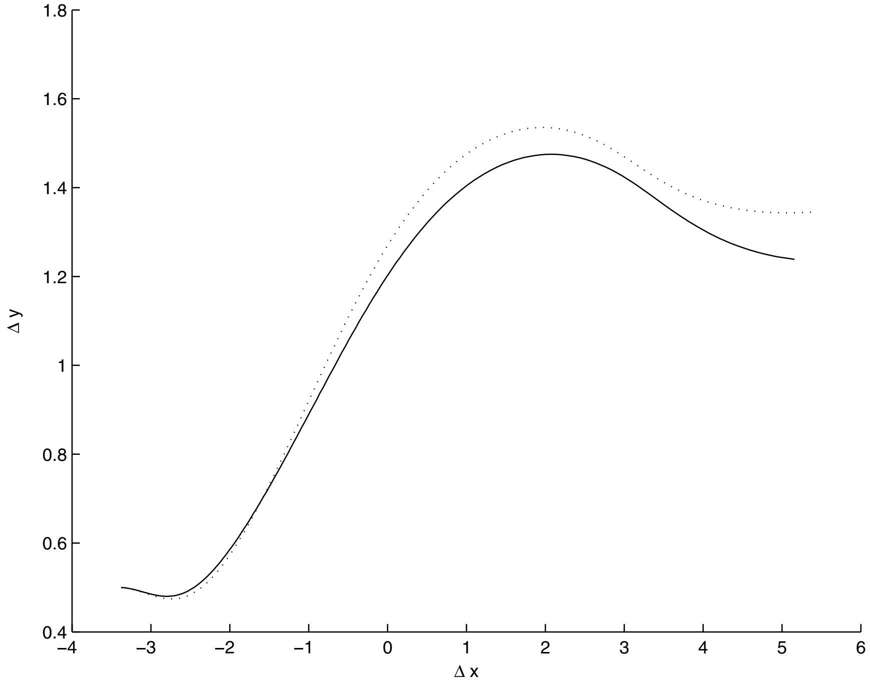

Fig. 3e. The difference, Δy, between the y-coordinates of the drop centroids plotted versus the difference, Δx, between the x-coordinates in the drop centroids for the simulation shown in Fig. 3a. Notation as in that figure.

flattening followed by the formation of a dimple. As the outer drops approach the two inner interacting drops, the lubrication forces cause the leading edge of the outer drops to bend and roughly align with the inner drops. The bend is a precursor of the dimple that develops in the outer drops as all four drops interact. At later times, the inner drops broaden and the outer drops elongate to eventually span both inner drops. The drop morphologies are quite complex as the drops try to squeeze past one another. Note that the presence of the outer drops serves to confine the inner drop interaction leading to an overall compression of the drop morphologies.

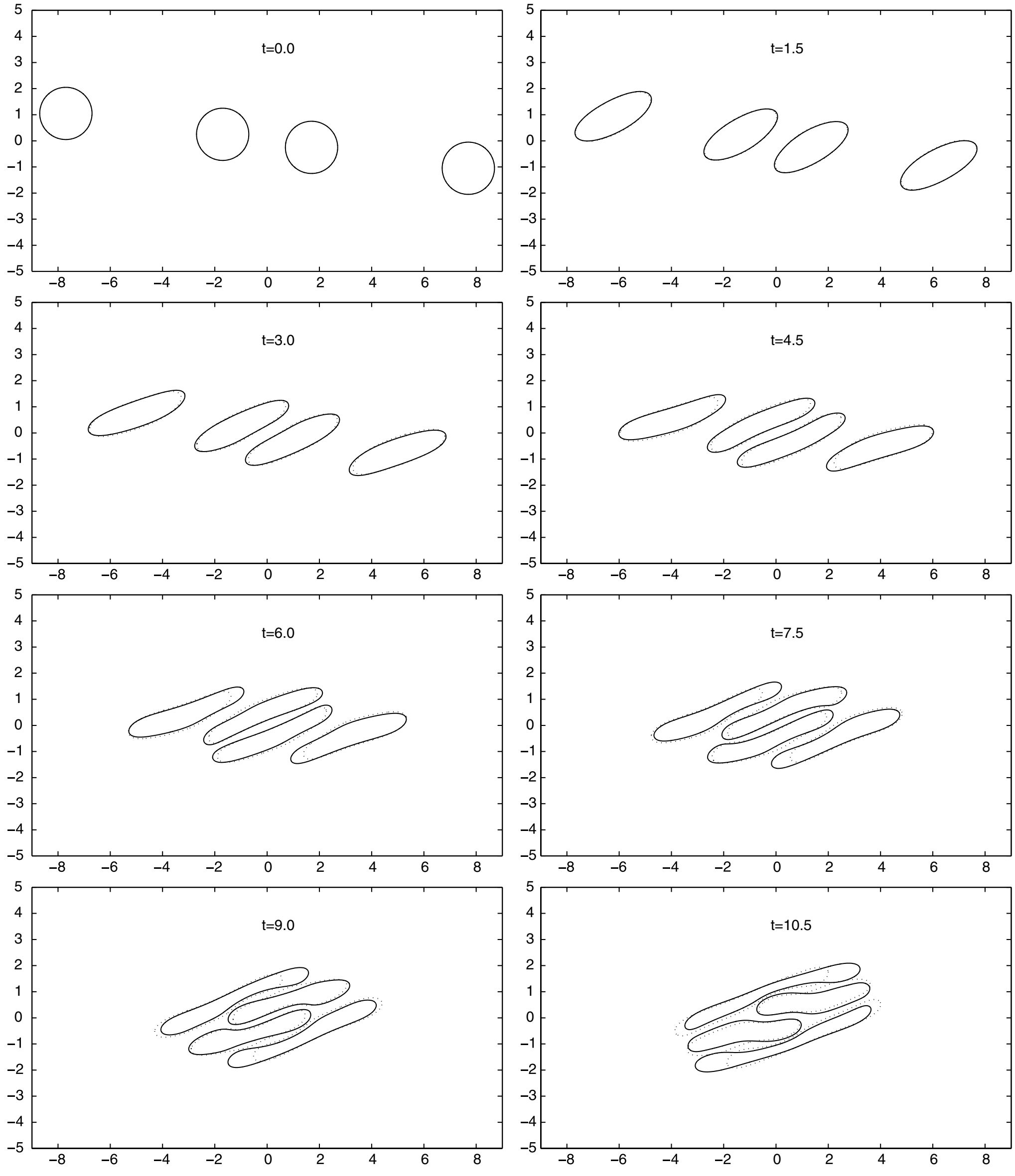

Fig. 4a. Morphologies of four drops in shear flow with $Ca = 0.7$, nonlinear EOS (solid) with $E = 0.2$, $x = 0.3$ and $Pe = 10$. Dotted: $x = 0$ (no surfactant). Times range from $t = 0$ to 10.5 in increments of 1.5.

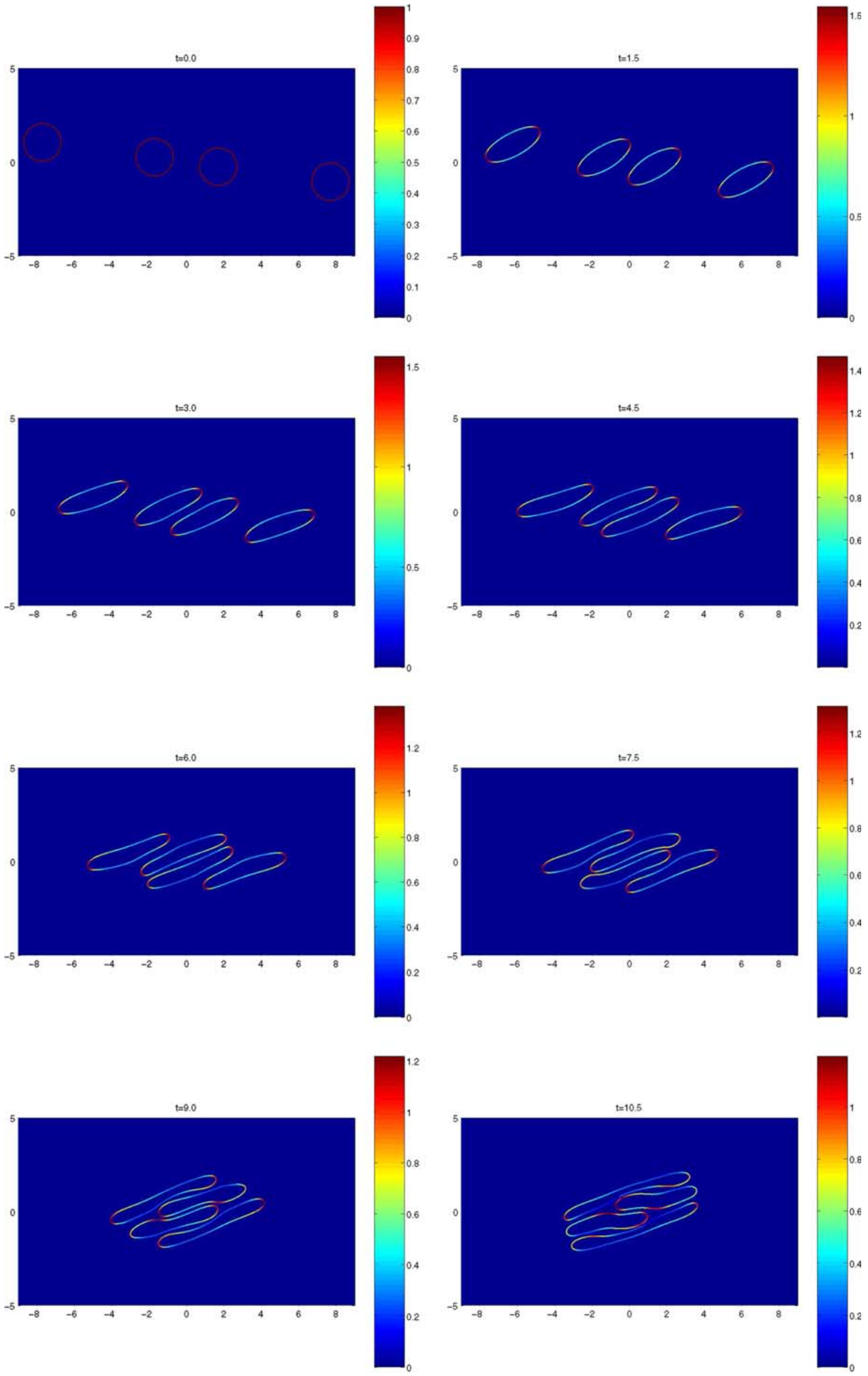

Fig. 4b. Surfactant distribution for the simulation shown in Fig. 4c. Times and parameters as in that figure.

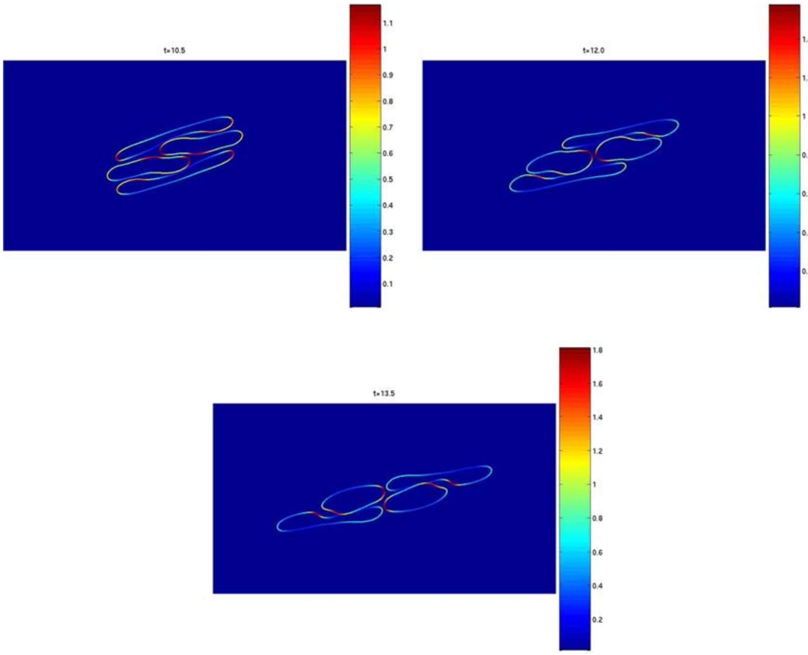

Fig. 4c. Surfactant distribution obtained using different level-set and surfactant concentration functions on each interface, and also imposing symmetry, for the continuation of the simulation shown in Fig. 4. The parameters as in that figure. Times shown are $t = 10.5$, 12.0 and 13.5.

The effect of surfactant on the morphologies is more significant than in the other cases we have considered in Sections 4.1 and 4.2. The surfactant laden inner drops have significantly narrower and more rotated leading edges than do their clean counterparts. The surfactant laden outer drops are more stretched, particularly on the leading edges, than the corresponding clean drops.

In Fig. 4b, the surfactant distribution is shown on the drop interfaces. During the initial stages of the interaction of the two inner drops, the surfactant distribution on the inner drops is similar to that obtained in Section 4.2 for isolated two-drop interactions. By time $t = 9.0$, the surfactant on the inner drops becomes concentrated near the regions of closest approach which are not the flat regions but are near the trailing-edge drop-tips and the curved regions near the leading edges. At time $t = 10.5$, the regions of high surfactant concentration in the curved regions of the inner drops moves toward the trailing edge drop tip as the inner drops are separating. The surfactant distribution on the outer drops is beginning to resemble that on the inner drops at the earlier stages of interaction. These results suggest that the effects of surfactants are more pronounced and more complicated for interactions of multiple drops than for either single drop or interactions of two drops.

In the clean case, the drops smoothly squeeze past one another (not shown) at later times. However, at times slightly larger than 10.5, the algorithm with surfactant breaks down because the surface tension becomes negative at a point of large surfactant concentration. Refining the time step did not significantly alleviate this difficulty. Computational costs prevented us from refining the spatial grid size further. We believe the breakdown of the surfactant simulation is due to a lack of spatial resolution in the near contact region between the inner and outer drops. This can be solved by increasing local resolution by using local mesh refinement. The development of adaptive mesh refinement by using overlapping patches of Cartesian meshes following the methodology in [7] is currently under study.

Another possible remedy we are pursuing is the use of different level-set functions and surfactant concentration functions for each interface. This is discussed further in Section 5 and a preliminary result of such an approach is shown in Fig. 4c. It is known that the use of single surfactant concentration and level-set functions to described multiple interfaces may lead to numerical difficulties in extending these functions off the interfaces in near contact regions. For example, e.g., see [40], extensions of the level-set function off interfaces may lead to poorly behaved discretizations of the interface curvature in regions of near contact. Since the discretization of the surfactant equation explicitly uses the interface curvature, see Eq. (30), this can cause the surfactant concentration to become inaccurate. In addition, the extension of f off the interface may analogously lead to non-smooth derivatives of f which can also lead to inaccuracy in both f and the Marangoni force. We are also studying the use of one-sided differencing of both the level-set function and the surfactant concentration in regions of near contact following the approach developed by Macklin and Lowengrub [40].

5. Conclusions

In this paper, we have presented a level-set method for the simulation of fluid interfaces with insoluble surfactant in two-dimensions. The method can be straightforwardly extended to three-dimensions and to soluble surfactants. The method couples the IIM for solving the fluid flow equations with a modification of scheme recently developed by Xu and Zhao [62] for the surfactant transport equation. Novel techniques were developed to accurately conserve component (domain) volume and surfactant mass during the evolution. Convergence of the method was demonstrated numerically and the method was applied to study the effects of surfactant on single drops, drop–drop interactions and interactions among multiple drops in Stokes flow under a steady applied shear. Due to Marangoni forces and to non-uniform Capillary forces, the presence of surfactant resulted in larger drop deformations and more complex drop–drop interactions compared to the analogous cases for clean drops. The effects of surfactant were found to be most significant in flows with multiple drops. To our knowledge, this is the first time that the level-set method has been used to simulate fluid interfaces with surfactant.

There are a number of future directions that should be pursued. The methods should be extended to three dimensions and the effect of viscosity ratio on the evolution should be considered. In addition, surfactant solubility as well as finite Reynolds number flows should also be investigated. From the numerical side, one of the most significant issues to be addressed is increasing the accuracy of interactions among many drops in multiphase flows. This is particularly evident from the simulation of four drops in Fig. 4, where the surface tension becomes negative and the simulation breaks down. In this simulation, the computational constraints associated with using a uniform Cartesian mesh prevent us from achieving the resolution required to accurately simulate the drop interactions. To overcome this difficulty, adaptive mesh refinement strategies should be employed.

Another strategy that could be pursued is the use of different level-set and surfactant-concentration functions for each interface. That is, instead of using one function to describe the drop morphologies, four level-set functions could be used to describe the fluid morphology. The algorithm presented in this paper could then be used to simulate the evolution where the surface forces are obtained by summing the contributions from each drop. Using this strategy, in addition to enforcing symmetry in the flow, we are able to continue the simulation beyond the previous breakdown time $t = 10.5$ (in Figs. 4a and 4b) and the result is shown in Fig. 4c. However, using this strategy at later times becomes problematic because the drops interact only through the flow. As a result, the drops eventually overlap one another (rather than coalescing) leading to an unphysical configuration. To overcome this drawback in a general way, hydrodynamic repulsion forces (e.g., lubrication forces) could be introduced to prevent drop overlap. In addition, a locally adaptive mesh should also be used to better resolve the near contact regions. This is currently under study.

Acknowledgements

The authors thank Mike Siegel and Vittorio Cristini for helpful discussions. The authors acknowledge the support of the Network and Academic Computing Services at the University of California, Irvine. The authors also thank the computing facilities of the Department of Mathematics and the Department of Biomedical Engineering at the University of California, Irvine. J. Xu acknowledges the support of a PIMS fellowship. Z. Li was partially supported by NSF grants DMS-0201094 and DMS-0412654, and by an ARO Grant 39676-MA. J. Lowengrub acknowledges the support of the National Science Foundation, Division of Mathematical Sciences. H. Zhao is partially supported by an ONR Grant N00014-02-1-0090, a DARPA Grant N00014-02-1-0603 and a Sloan Foundation Fellowship.

References

[1] D. Adalsteinsson, J.A. Sethian, The fast construction of extension velocities in level set methods, J. Comput. Phys. 148 (1999) 2–22.

[2] D. Adalsteinsson, J.A. Sethian, Transport and diffusion of material quantities on propagating interfaces via level set method. Preprint, 2002.

[3] D. Anderson, G. McFadden, A. Wheeler, Diffuse interface methods in fluid mechanics, Ann. Rev. Fluid Mech. 30 (1988) 139.

[4] E. Aulisa, S. Manservisi, R. Scardovelli, A mixed markers and volume-of-fluid method for the reconstruction and advection of interfaces in two-phase and free-boundary flows, J. Comput. Phys. 188 (2003) 611.

[5] H.D. Ceniceros, The effects of surfactants on the formation and evolution of capillary waves, Phys. Fluids 15 (2003) 245–256.

[6] S. Chen, B. Merriman, S. Osher, P. Smereka, A simple level set method for solving Stefan problems, J. Comput. Phys. (1997).

[7] P. Colella, D.T. Graves, T.J. Ligocki, D.F. Martin, D. Modiano, D.B. Serafini, B. Van Straalen, Chombo Software Package for AMR Applications, Appl. Num. Alg. Group, NERSC Division, Lawrence Berkeley National Laboratory, Berkeley, CA, 2003.

[8] V. Cristini, J. Blawzdziewicz, M. Loewenberg, An adaptive mesh algorithm for evolving surfaces: simulations of drop breakup and coalescence, J. Comput. Phys. 168 (2001) 445–463.

[9] R. Defay, I. Priogine, Surface Tension and Adsorption, Wiley, New York, 1966.

[10] M.A. Drumwright-Clarke, Y. Renardy, The effect of insoluble surfactant at dilute concentration on drop breakup under shear with inertia, Phys. Fluids 16 (2004) 14.

[11] C.D. Eggleton, T.-M. Tsai, K.J. Stebe, Tip streaming from a drop in the presence of surfactants, Phys. Rev. Lett. 87 (2001) 048302.

[12] D. Enright, R. Fedkiw, J. Ferziger, I. Mitchell, A hybrid particle level set method for improved interface capturing, J. Comput. Phys. 183 (2002) 83–116.

[13] R. Fedkiw, T. Aslam, B. Merriman, S. Osher, A nonoscillary Eulerian approach to interfaces in multimaterials flows (the ghost fluid method), J. Comput. Phys. 152 (1999) 457–492.

[14] F. Gibou, R. Fedkiw, A fourth order accurate discretization for the laplace and heat equations on arbitrary domains with applications to the Stefan problem, J. Comput. Phys. 202 (2005) 577.

[15] J. Glimm, J.W. Grove, X.L. Li, K.-M. Shyue, Q. Zhang, Y. Zeng, Three-dimensional front tracking, SIAM J. Sci. Comput. 19 (1998) 703.

[16] J. Goerke, Pulmonary surfactant: functions and molecular composition, Biochim. Biophys. Acta 1408 (1998) 79.

[17] B.T. Helenbrook, L. Martinelli, C.K. Law, A numerical method for solving incompressible flow problems with a surface of discontinuity, J. Comput. Phys. 148 (1999) 366.

[18] S.E. Hieber, J.H. Walther, P. Koumoutsakos, Remeshed smoothed particle hydrodynamics simulation of the mechanical behavior of human organs, Technol. Health Care 12 (2004) 305.

[19] T.Y. Hou, Z. Li, S. Osher, H. Zhao, A hybrid method for moving interface problems with applications to the Hele–Shaw flows, J. Comput. Phys. 134 (1997) 236.

[20] T.Y. Hou, J.S. Lowengrub, M.J. Shelley, Boundary integral methods for multicomponent fluids and multiphase materials, J. Comput. Phys. 169 (2001) 302.

[21] A.J. James, J. Lowengrub, A surfactant-conserving volume-of-fluid method for interfacial flows with insoluble surfactant, J. Comput. Phys. 201 (2004) 685–722.

[22] Y.-J. Jan, G. Tryggvason, Computational studies of contaminated bubbles, in: I. Sahin, G. Tryggvason (Eds.), Proceedings of a Symposium on the Dynamics of Bubbles and Vorticity Near Free Surfaces, vol. 46, ASME, 1991.

[23] G.-S. Jiang, D. Peng, Weighted eno schemes for Hamilton–Jacobi equations, SIAM J. Sci. Comput. 21 (2000) 2126.

[24] G.-S. Jiang, C.-W. Shu, Efficient implementation of weighted ENO schemes, J. Comput. Phys. 126 (1996) 202–228.

[25] J.S. Kim, K.K. Kang, J.S. Lowengrub, Conservative multigrid methods for Cahn–Hilliard fluids, J. Comput. Phys. 193 (2004) 511.

[26] J.S. Kim, J. Lowengrub, Interfaces and Multicomponent Fluids, Encyclopedia for Math and Physics, Elsevier, to appear, 2005.

[27] M. Lai, Z. Li, A remark on jump conditions for the three-dimensional Navier–Stokes equations involving an immersed moving membrane, Appl. Math. Lett. 14 (2001) 149.

[28] L.D. Landau, E.M. Lifshitz, Fluid Mechanics, Pergamon Press, New York, 1958.

[29] L.G. Leal, Flow induced coalecsence of drops in a viscous fluid, Phys. Fluids 16 (2004) 1833.

[30] L. Lee, R. LeVeque, An immersed interface method for incompressible Navier–Stokes equations, SIAM J. Sci. Comput. 25 (2003) 832.

[31] R. LeVeque, Z. Li, The immersed interface method for elliptic equations with discontinuous coefficients and singular sources, SIAM J. Numer. Anal. 31 (1994) 1019–1044.

[32] R. LeVeque, Z. Li, Immersed interface methods for stokes flow with elastic boundaries or surface tension, SIAM.J. Sci. Comput. 18 (1997) 709.

[33] X. Li, C. Pozrikidis, Effect of surfactants on drop deformation and on the rheology of dilute emulsion in stokes flow, J. Fluid Mech. 385 (1999) 79–99.

[34] Z. Li, The immersed interface method – a numerical approach for partial differential equations with interfaces. PhD Thesis, University of Washington, Seattle, 1994.

[35] Z. Li, K. Ito, Maximum principle preserving schemes for interface problems with discontinuous coefficients, SIAM J. Sci. Comput. 23 (2001) 339–361.

[36] Z. Li, K. Ito, M-C. Lai, An augmented approach for Stokes equations with discontinuous viscosity and singular forces, NCSU Tech. Reports: CRSC-TR04-24.

[37] Z. Li, M. Lai, The immersed interface method for the Navier–Stokes equations with singular forces, J. Comput. Phys. 171 (2001) 822.

[38] X. Liu, R. Fedkiw, M. Kang, A boundary condition capturing method for Poisson's equation on irregular domains, J. Comput. Phys. 160 (2000) 151.

[39] M. Loewenberg, E.J. Hinch, Collision of two deformable drops in shear flow, J. Fluid Mech. 388 (1997) 299.

[40] P. Macklin, J. Lowengrub, Evolving interfaces via gradients of geometry-dependent interior Poisson problems: application to tumor growth, J. Comput. Phys. 203 (2005) 191.

[41] W.J. Milliken, H.A. Stone, L.G. Leal, The effect of surfactant on transient motion of Newtonian drops, Phys. Fluids A 5 (1993) 69.

[42] N.R. Morrow, G. Mason, Recovery of oil by spontaneous imbibition, Curr. Opin. Coll. Int. Sci. 6 (2001) 321.

[43] S. Osher, R.P. Fedkiw, Level set methods: an overview and some recent results, J. Comput. Phys. 169 (2001) 463.

[44] S. Osher, J.A. Sethian, Fronts propagating with curvature dependent speed: algorithms based on Hamilton–Jacobi formulations, J. Comput. Phys. 79 (1988) 12.

[45] Y. Pawar, K.J. Stebe, Marangoni effects on drop deformation in an extensional flow: the role of surfactant physical chemistry. I. Insoluble surfactants, Phys. Fluids 8 (1996) 1738.

[46] D. Peng, B. Merriman, S. Osher, H.-K. Zhao, M. Kang, A PDE-based fast local level set method, J. Comput. Phys. 155 (1999) 410.

[47] C.S. Peskin, The immersed boundary method, Acta Numer. (2002) 1.

[48] C. Pozrikidis, Interfacial dynamics for Stokes flows, J. Comput. Phys. 169 (2001) 250.

[49] Y.Y. Renardy, M. Renardy, V. Cristini, A new volume-of-fluid formulation for surfactants and simulations of drop deformation under shear at a low viscosity ratio, Eur. J. Mech. B 21 (2002) 49–59.

[50] R. Scardovelli, S. Zaleski, Direct numerical simulation of free-surface and interfacial flow, Ann. Rev. Fluid Mech. 31 (1999) 567.

[51] J.A. Sethian, P. Smereka, Level set methods for fluid interfaces, Ann. Rev. Fluid Mech. 35 (2003) 341.

[52] S. Shin, D. Juric, Modeling three-dimensional multiphase flow using a level contour reconstruction method for front tracking without connectivity, J. Comput. Phys. 180 (2002) 427.

[53] C.-W. Shu, Total-variation-diminishing time discretization, SIAM J. Sci. Stat. Comput. 9 (1988) 1073.

[54] H.A. Stone, A simple derivation of the time-dependent convective-diffusion equation for surfactant transport along a deforming interface, Phys. Fluids A 2 (1989) 111.

[55] H.A. Stone, L.G. Leal, The effects of surfactants on drop deformation and breakup, J. Fluid Mech. 220 (1990) 161.

[56] M. Sussman, A second order coupled level-set and volume-of-fluid method for computing growth and collapse of vapor bubbles, J. Comput. Phys. 187 (2003) 110.

[57] M. Sussman, E. Fatemi, P. Smereka, S. Osher, An improved level set method for incompressible two-phase flows, Comput. Fluids 277 (1998) 663–680.

[58] M. Sussman, E. Puckett, A coupled level-set and volume-of-fluid method for computing 3D axisymmetric incompressible two-phase flows, J. Comput. Phys. 162 (2000) 301.

[59] M. Sussman, P. Smereka, S. Osher, A level set approach for computing solutions to incompressible two-phase flow, J. Comput. Phys. 114 (1994) 146–159.

[60] G. Tryggvason, B. Bunner, A. Esmaeeli, D. Juric, N. Al-Rawahi, W. Tauber, J. Han, S. Nas, Y.-J. Jan, A front tracking method for the computations of multiphase flow, J. Comput. Phys. 169 (2001) 708.

[61] H. Wong, D. Rumschitzki, C. Maldarelli, On the surfactant mass balance at a deforming fluid interface, Phys. Fluids 8 (1996) 3203.

[62] J. Xu, H. Zhao, An Eulerian formulation for solving partial differential equations along a moving interface, J. Sci. Comput. 19 (2003) 573–594.

[63] S. Yon, C. Pozrikidis, A finite-volume/boundary-element method for flow past interfaces in the presence of surfactants, with application to shear flow past a viscous drop, Comput. Fluids 27 (1998) 879.

[64] P. Yue, J.L. Feng, C. Liu, J. Shen, A diffuse-interface method for simulating two-phase flows of complex fluids, J. Fluid Mech. 515 (2004) 293.

[65] H. Zhao, T.F. Chan, B. Merriman, S. Osher, A variational level set approach to multiphase motion, J. Comput. Phys. 127 (1996) 179–195.